JGR Biogeosciences

RESEARCH ARTICLE
10.1029/2020JG005924

Key Points:
- Soil CO_2 observations are used to drive a model of depth-resolved respiration in a montane meadow
- Precipitation timing relative to plant phenologic stage controls episodic and seasonal soil CO_2 fluxes
- Subsoil processes including weathering and deep CO_2 sources all contribute to observed surface fluxes

Supporting Information:
- Supporting Information S1

Correspondence to:
M. J. Winnick,
mwinnick@umass.edu

Citation:
Winnick, M. J., Lawrence, C. R., McCormick, M., Druhan, J. L., & Maher, K. (2020). Soil respiration response to rainfall modulated by plant phenology in a montane meadow, East River, Colorado, USA. *Journal of Geophysical Research: Biogeosciences*, *125*, e2020JG005924. https://doi.org/10.1029/2020JG005924

Received 23 JUN 2020
Accepted 24 SEP 2020
Accepted article online 12 OCT 2020

©2020. American Geophysical Union. All Rights Reserved.

Soil Respiration Response to Rainfall Modulated by Plant Phenology in a Montane Meadow, East River, Colorado, USA

Matthew J. Winnick[1,2], Corey R. Lawrence[3], Maeve McCormick[2], Jennifer L. Druhan[4], and Kate Maher[2,5]

[1]Department of Geosciences, University of Massachusetts Amherst, Amherst, MA, USA, [2]Department of Earth Systems Science, Stanford University, Stanford, CA, USA, [3]U.S. Geological Survey, Geosciences and Environmental Change Science Center, Denver, CO, USA, [4]Department of Geology, University of Illinois at Urbana-Champaign, Champaign, IL, USA, [5]Rocky Mountain Biological Laboratory, Gothic, CO, USA

Abstract Soil respiration is a primary component of the terrestrial carbon cycle. However, predicting the response of soil respiration to climate change remains a challenge due to the complex interactions between environmental drivers, especially plant phenology, temperature, and soil moisture. In this study, we use a 1-D diffusion-reaction model to calculate depth-resolved CO_2 production rates from soil CO_2 concentrations and surface efflux observations in a subalpine meadow in the East River watershed, CO. Modeled rates are compared to in situ soil temperature and moisture conditions and MODIS satellite enhanced vegetation index (EVI) representing plant phenology across three hydrologically distinct growing seasons from 2016–2018. While soil respiration correlated with temperature on diel timescales ($p < 0.05$), seasonal variability was dominated by soil moisture and plant phenology ($p < 0.05$). We observed significant respiration increases in response to precipitation events; however, magnitude and duration were significantly higher in 2017 than 2016 despite similar wetting characteristics. Based on MODIS EVI, we suggest that the respiration response to rainfall is controlled by plant phenology, which in turn reflects the capacity of plants to respond to precipitation via increased photosynthesis and autotrophic respiration, behavior that is not captured in typical soil respiration pulse models. Projected changes in montane climate such as earlier snowmelt and prolonged fore-summer drought may decrease soil respiration fluxes by decreasing the overlap between peak productivity and the summer monsoon. Finally, we observed significant late season CO_2 fluxes from the deep subsoil (>165 cm) that support growing evidence for the importance of subsoil processes in driving integrated respiration fluxes.

1. Introduction

Fluxes of CO_2 to the atmosphere from soil respiration represent one of the primary components of the terrestrial carbon cycle, acting to offset CO_2 uptake from the atmosphere by photosynthesis (Raich & Schlesinger, 1992). Globally, soil respiration fluxes are roughly an order of magnitude higher than anthropogenic emissions; as such, modest changes in the balance between this efflux and photosynthetic carbon uptake have the potential to significantly amplify or dampen anthropogenic climate change. Thus, predicting the response of soil respiration to environmental change is paramount to forecasting future carbon cycle dynamics and remains one of the largest uncertainties in current climate projections (Ciais et al., 2013; Friedlingstein et al., 2006; Heimann & Reichstein, 2008).

Montane ecosystems are especially vulnerable to changing climate as a result of the amplification of atmospheric warming at higher elevation (Bradley et al., 2004; Diaz et al., 2003; MRI, 2015). In particular, warming has the potential to alter high-elevation hydrology in the U.S. Rocky Mountains by reducing winter snowpack and increasing evaporative demand, leading to longer growing seasons and increasing drought length and severity between snowmelt and the arrival of summer monsoon precipitation (Knowles et al., 2006; Mote et al., 2005). A number of studies have shown the potential for impacts on ecosystem carbon dynamics and soil respiration fluxes. Primary productivity in Rocky Mountain ecosystems historically decreases in response to earlier snowmelt and reduced snowpack (Knowles et al., 2018; Monson et al., 2005) and the severity and duration of summer drought (Berkelhammer et al., 2017; Sloat et al., 2015). Reduced

snowpack can also reduce wintertime soil respiration through decreases in shallow soil temperatures (Monson et al., 2006). However, the response of soil respiration to changes in montane hydrology during the growing season is less well constrained. In spite of increased temperatures, decreases in water availability could lead to reduced soil moisture and plant inputs of carbon to soils (e.g., Saleska et al., 1999, 2002).

Disentangling these dynamic and interacting drivers remains a unique challenge for characterizing soil respiration patterns across timescales. Soil respiration fluxes represent a combination of (1) contributions from the microbial respiration of soil organic carbon (SOC), termed heterotrophic respiration, and (2) plant-mediated respiration, including both cellular respiration by roots and microbial respiration of young organic matter (e.g., roots and root exudates), operationally defined here as autotrophic respiration. Autotrophic and heterotrophic respiration are both responsive to environmental drivers such as temperature and moisture conditions, though differences in underlying response mechanisms and timescales can result in complex soil respiration patterns (e.g., Boone et al., 1998; Pregitzer et al., 2000) as detailed below. Partitioning autotrophic and heterotrophic responses, often through ^{14}C-CO_2 measurements, is particularly challenging due to the potential for alternative soil CO_2 sources (calcite and organic carbon in sedimentary rocks) and cost prohibitive in terms of capturing high-frequency or long-timescale behavior. Alternatively, the monitoring of depth-resolved CO_2 production and surface CO_2 fluxes may provide important insights into autotrophic and heterotrophic response mechanisms when analyzed and compared across characteristic response timescales and depths (e.g., shallow soil: <30 cm vs. subsoil: >30 cm). In particular, while subsoil depths are more insulated from environmental variability relative to shallow soils, recent studies have shown the potential for deep soil processes to contribute to or detract from observed CO_2 surface fluxes (Sánchez-Cañete et al., 2018; Wan et al., 2018), though these processes remain poorly characterized.

In terms of environmental drivers, increasing temperature broadly results in increased heterotrophic respiration (e.g., Bond-Lamberty & Thomson, 2010). However, this relationship is complicated by the molecular complexity of soil carbon functional types combined with differing temperature sensitivities and soil carbon protection mechanisms, such as physical aggregates and mineral-organic associations (e.g., Davidson, Janssens, & You, 2006; Lehmann & Kleber, 2015). Autotrophic respiration can amplify the dependence of total soil respiration on temperature when peak growth corresponds with higher temperatures (Boone et al., 1998; Curiel Yuste et al., 2004; Reichstein et al., 2003). On diel timescales, however, offsets between autotrophic respiration and peak temperatures lead to hysteresis in relationships between temperature and overall soil respiration (DeForest et al., 2006; Gaumont-Guay et al., 2008; Oikawa et al., 2014; Savage et al., 2013; Tang et al., 2005). Thus, the amplification or dampening of soil respiration sensitivity to temperature depends on observational timescales. Less well studied are how asynchronous variations in temperature and phenology interact over longer (weekly to seasonal) timescales.

Soil moisture generally drives respiration rates via a parabolic relationship (e.g., Davidson et al., 1998; Grant & Rochette, 1994; Reichstein et al., 2003), in which respiration is limited at low moisture due to limited supply of dissolved organic matter (e.g., Davidson et al., 2012; Sihi et al., 2018) and active microbial populations (Manzoni et al., 2014) and at high moisture due to limitations on O_2 supply. Additionally, respiration responds transiently to pulsed wetting events with antecedent dry conditions (e.g., Birch, 1958). These event-based respiration responses may be significant components of integrated soil CO_2 fluxes in semiarid environments (Fan et al., 2015); however, the vast majority of studies on pulse responses have focused on heterotrophic respiration dynamics, neglecting the potential coupling of vegetative responses to moisture availability. The role of plants in regulating soil respiration responses to pulse wetting events remains a significant challenge for conceptual and quantitative models of soil CO_2 fluxes. Plant responses to episodic wetting events involve an increase in photosynthetic carbon assimilation followed by increases in root and rhizosphere respiration. Due to the temporal lag between photosynthetic assimilation and appearance of photosynthates in the rhizosphere (Carbone & Trumbore, 2007; Ekblad & Hogberg, 2001; Ekblad et al., 2005), autotrophic respiration responds to episodic wetting on timescales of days to weeks, in contrast to heterotrophic respiration, which responds on timescales of hours (Carbone et al., 2011). Few studies have evaluated the contributions of episodic autotrophic respiration to seasonally integrated soil respiration fluxes or characterized the conditions under which plants were able or unable to respond to pulsed wetting events.

Here we seek to address these knowledge gaps through the characterization of depth-resolved soil respiration trends across three growing seasons (2016–2018) in a subalpine meadow in the Rocky Mountains of

central Colorado, USA. Our primary questions are as follows: (1) How do temperature, precipitation, and plant activity drive patterns of growing season soil respiration across subdaily to interannual scales? (2) How do autotrophic responses to rain events drive variability and magnitude of growing season respiration? and (3) How do subsoil processes contribute to surface measured soil CO_2 fluxes? Given the short duration of montane growing seasons and the importance of summer precipitation for plant productivity in the months following snowmelt, we hypothesized that precipitation amount and timing relative to plant phenology (i.e., the ability of plants to increase photosynthesis following rain events) is a primary driver of the magnitude and variability of growing season soil respiration fluxes in Rocky Mountain ecosystems.

To interrogate these questions, we used subsurface measurements of pCO_2 to calculate depth-resolved changes in net CO_2 production using a diffusion-reaction model and compare differences in respiration responses to environmental drivers including summer monsoon precipitation events within and across three growing seasons. Notably, this depth resolution allows us to assess the importance of processes occurring below the upper layers of soil, such as CO_2 fluxes into and out of the deep subsoil and to fingerprint hotspots of CO_2 production and consumption that may aid in the distinction of autotrophic and heterotrophic respiration responses.

2. Site Description

Depth-resolved soil pCO_2 data were collected within the upper East River watershed located in Gothic, Colorado (Figure 1). The East River watershed is considered broadly representative of many snowmelt-dominated headwater catchments in the Rocky Mountains (Markstrom et al., 2012). Our study site, Bradley Meadow (BM), is located on a hillslope that feeds into Bradley Creek—a minor tributary of the East River (*Lat:* 38.9871, *Lon:* −107.004). It is situated roughly 3 km north of the Rocky Mountain Biological Laboratory (RMBL) and resides within the Lawrence Berkeley National Laboratory's Watershed Science Focus Area (LBNL SFA; Hubbard et al., 2018). Site elevation is 2,970 m, roughly 600 m below tree line, with a slope of ~10° and aspect of ~115°. The vegetation, aspect, and elevation are comparable to the "moist zone" of the "Warming Meadow" climate manipulation experiment that ran from 1991 to 2019 (Harte, 2019; Saleska et al., 2002). Annual average temperatures are ~0°C, and daytime averages range from 19.4°C in July to −1.1°C in December based on a proximal, higher elevation weather station (3,261 m). Annual average precipitation at a proximal SNOTEL site (Schofield, Figure 1) is ~1,200 mm/year ± 230 with roughly 70% falling as snow during the winter.

Vegetation is characterized as a lower subalpine plant community comprising mostly long-lived perennials. The dominant herbaceous plant species adjacent to our measurement locations are *Delphiniun barberi*, *Potentilla pulcherrima*, *Erigeron speciosus*, *Ligusticum porteri*, and *Lathyrus lanszwertii var. leucanthus*, with ~20% undifferentiated graminoids. *Veratrum californicum* is found in scattered clusters across the hillslope. Average aboveground biomass at the end of the 2016 growing season, measured by destructive harvest, was 331 g/m^2 (Hsu et al., 2018).

Hydroclimate in the region is characterized by snowmelt in the late spring/early summer, with first snow-free days varying from May to July (Figure 2a). Relatively little precipitation occurs during June, a period termed the fore-summer drought. The onset of the North American summer monsoon in July and August contributes additional precipitation during the growing season, though the relative importance of snowmelt versus monsoonal moisture for plant productivity is a topic of ongoing research (Knowles et al., 2018; Sloat et al., 2015). Within our observational period, peak snow water equivalents (SWEs) for 2016, 2017, and 2018 at the Schofield SNOTEL site were 0.71, 1.27, and 0.74 m, respectively, compared to an average of 0.97 m for 1986–2018 (Figure 2b). The first snow-free days in our 3 year consecutive period occurred on days of year (DOYs) 163, 169, and 150, respectively, compared to an average of 163 for 1986–2018. In 2016, the summer growing season was relatively dry, consisting of scattered small precipitation events in June and July, followed by a large monsoonal event in late August (Figure 2a). In 2017, a large monsoonal event occurred in mid-July, with 50% of June, July, August (JJA) precipitation occurring within a 1 week span from 13 July to 19 July. In 2018, relatively little precipitation fell during the growing season, with a few small events scattered throughout July and August. In general, 2016 provided a reasonable representation of average conditions over the past 32 years, 2017 was a relatively wet year, and 2018 was a relatively dry year.

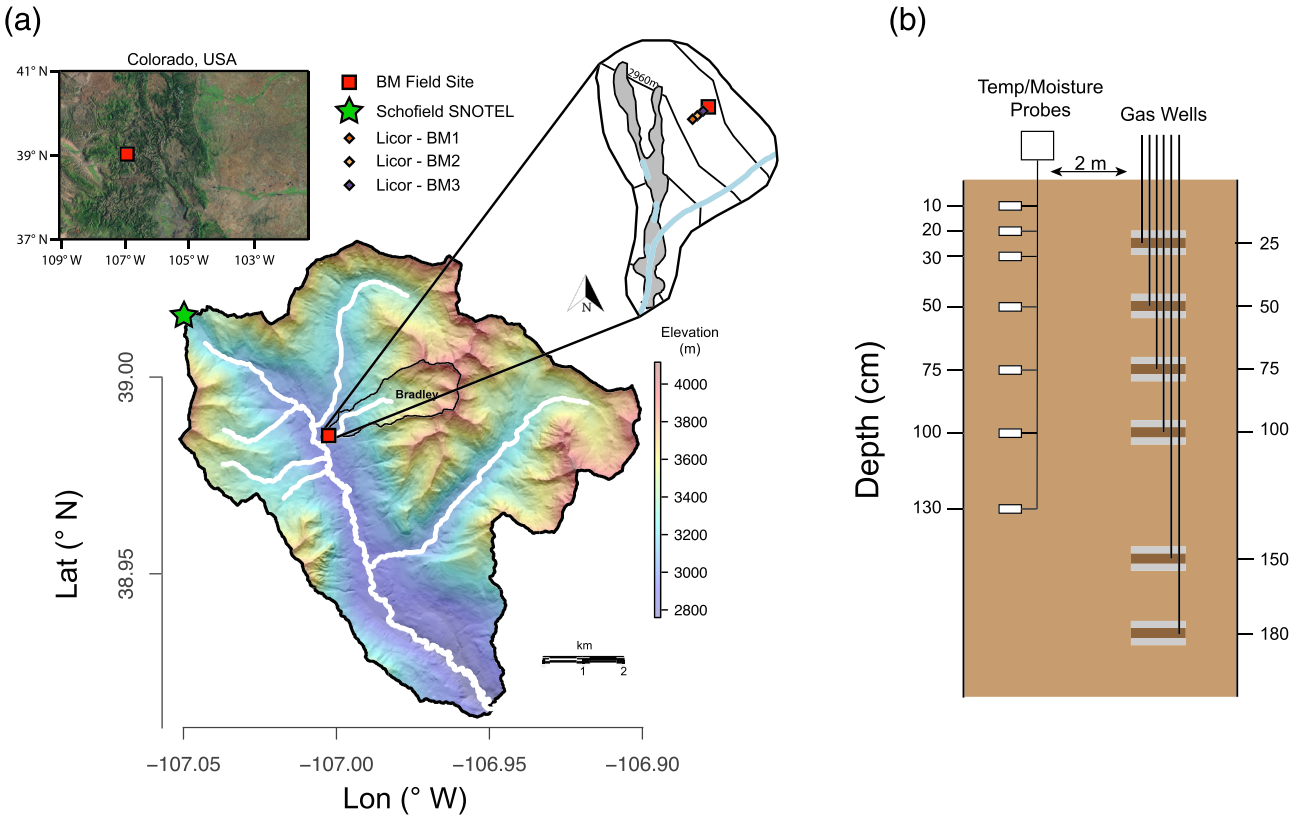

Figure 1. (a) Location of Bradley Meadow (BM) site installation within the East River watershed and Schofield SNOTEL site, Gunnison County, CO (see state map at top). BM inset map displays riparian area (gray shading) and 10 m elevation contour lines. LI-COR sites along hillslope represent location of autochambers described in section 3.1. (b) Bradley Meadow field monitoring installation showing arrays of Campbell CS-655 reflectometer probes (left) and stainless-steel gas well arrays (right). Gas wells are embedded in a layer of carbonate-free sand between impermeable bentonite layers.

The site is underlain by the calcareous Cretaceous Mancos Shale, composed primarily of quartz, clay minerals, calcium carbonate, pyrite, and shale organic matter (Morrison et al., 2012). Soils at BM extend to a depth of ~1 m above weathered shale saprolite and are classified as Typic Cryoborolls. The texture is silty clay near the surface, grading to clay at ~0.6 m. At a depth of 1 m, coarse rock fragments were encountered, and below this depth, the shale saprolite takes on a darker color with moist and clayey texture. A semiquantitative assessment of root distributions indicated visible fine roots to approximately the depth of the saprolite interface at 1 m (Lawrence, unpublished). Previous work has shown that weathering fluxes are dominated by carbonate dissolution reflecting a balance of soil-respired CO_2 in the shallow subsurface and pyrite oxidation in the deeper subsurface (Carroll et al., 2018; Winnick et al., 2017).

Previous studies of BM soils have characterized the amount and speciation of organic carbon content through combined TC-EA, F-TIR, and XAS analyses (Hsu et al., 2018). Organic carbon content in the soil profile decreases from ~2.5% by mass near the surface (0–30 cm) to ~1% by mass at 105 cm. Calcium carbonate is present (1–3% by mass) at depths below ~40 cm. SOC primarily reflects polysaccharide and carbonyl functional groups, similar to the composition of litter inputs (Hsu et al., 2018). Additionally, incubated heterotrophic respiration was extremely sensitive to pulsed wetting, showing increased rates that peaked between 5 and 24 hr after wetting (Liu et al., 2019).

3. Methods

3.1. Soil Monitoring

In November 2015, a nested gas well array was installed at the BM site, consisting of six wells constructed of stainless-steel tubing with a 60 μm mesh screen attached to the buried end and a compression fitting at

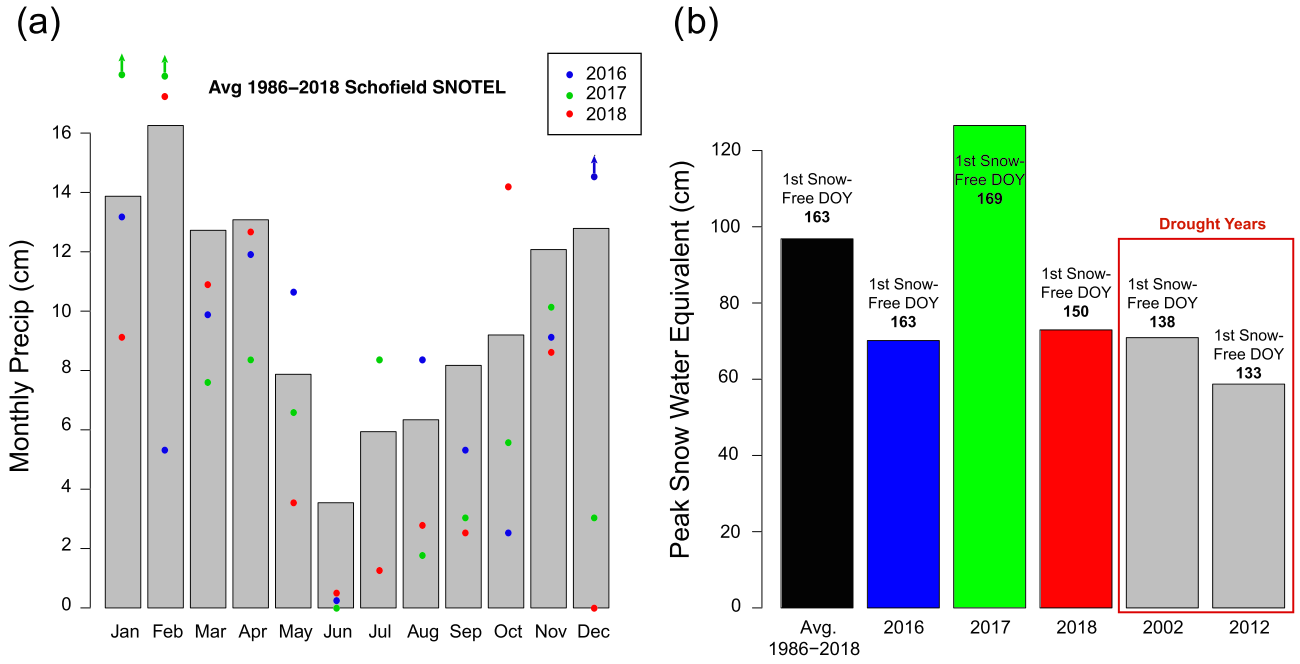

Figure 2. Hydroclimatology from Schofield SNOTEL site showing (a) average monthly precipitation for 1986–2018 with colored points representing monthly values for 2016–2018 over our observation period and (b) peak snow water equivalent and first snow-free day for 1986–2018 average, individual years 2016–2018, and historical drought years 2002 and 2012.

the surface end. Gas wells were installed to depths of 25, 50, 75, 100, 130, and 180 cm, spanning the depth to which a hand auger could penetrate. Each gas well was buried within an ~4 cm layer of carbonate-free sand between two layers of bentonite clay (Figure 1b). In June 2016 we installed a series of factory-calibrated Campbell CS-655 soil water content reflectometers for measuring temperature and volumetric water content (VWC) connected to a Campbell 200x data logger (Campbell Scientific, Logan, UT, USA), roughly 2 m from the existing gas wells (Figure 1b). Data were logged at intervals of 1 to 6 hr over the course of the monitoring period.

Gas samples were pulled from wells using gas tight syringes after clearing roughly twice the volume of tubing. Soil gas pCO_2 was measured by direct injection of gas samples to a field-portable infrared gas analyzer (IRGA) unit (EGM-5, PP Systems, Amesbury, MA, USA). For each gas sample, 60 ml of gas was pulled from the well, and 30 ml was injected into the IRGA. Measured pCO_2 was taken as the maximum measured values during injection, and results were corrected based on lab calibration with GASCO standards (Gasco Affiliates, LLC., Oldsmar, FL, USA) ranging in concentration from 400–25,000 ppm, with typical triplicate measurement standard deviations of ±5%. Surface soil CO_2 fluxes were measured, typically in triplicate, during each field visit through a soil respiration chamber (PP Systems, SRC-2), and reported values represent the average of these triplicates. Flux measurement uncertainty based on triplicate measurements was ±8%.

Sampling took place on a roughly weekly basis between June and October 2016, 2017, and 2018. However, sampling frequency and date ranges between years were variable due to the remote location and weather dependence of access. Over three seasons, 52 pCO_2 profiles were measured composing 312 individual pCO_2 measurements.

Additionally, during June 2017, a LI-COR 8100 soil flux system (LI-COR Biosciences, Lincoln, NE, USA) with three automated respiration chambers was installed along the hillslope to measure diel variation in soil respiration fluxes (Figure 1b). Two chambers (BM-2 and BM-3) were situated in vegetation similar to that of the gas well array, while BM-1 was placed within a cluster of *Veratrum californicum*. The unit collected ~9 days of hourly data in triplicate from each chamber but failed with the onset of monsoonal storms in July 2017.

3.2. Diffusion-Production Model

To resolve soil respiration processes with depth, we used soil pCO_2 measurements along with temperature, VWC, and surface CO_2 fluxes to constrain a 1-D diffusion-reaction model of CO_2 across the soil profile. This methodology has been used extensively in previous studies (e.g., Davidson, Savage, et al., 2006; Davidson & Trumbore, 1995; Tang et al., 2003). In this model, CO_2 concentrations change through time as a function of diffusive transport and net production (+)/consumption (−), as

$$\frac{dC}{dt} = D^* \left(\frac{d^2C}{dz^2}\right) + P \tag{1}$$

where C is the concentration of CO_2 (mol/cm^3), D^* is effective diffusivity (cm^2/s), and P is net production rate (mol/cm^3/s) incorporating both respiration and CO_2 drawdown via aqueous advective transport and weathering. The interval between our sampling trips varied from 1–30 days, and we make the simplifying assumption that each pCO_2 profile represents steady-state conditions ($dC/dt = 0$) so that net production can be solved as

$$P = -D^* \left(\frac{d^2C}{dz^2}\right) \tag{2}$$

We also solve a transient version of this model; however, as average offsets in calculated production rates are <0.002 $gCO_2/m^2/hr$ between the steady-state and transient models (supporting information), we use the simpler steady-state version here. To apply our measurements to this modeling framework, we used a first-order centered difference approximation such that the second derivative of C at location i (C_i) is

$$\frac{d^2C_i}{dz^2} = \frac{C_{i+1} - 2C_i + C_{i-1}}{\Delta z^2} \tag{3}$$

where Δz is the depth interval between measurements. In the case of irregular depth spacings, we linearly interpolated concentration and diffusivity data to a uniform spacing of 25 cm and reinterpolated the calculated production results to measured grid spacing.

Boundary conditions were prescribed using the pCO_2 of the atmosphere (450 ± 25 ppm based on typical EGM-5 readings over the course of the three seasons) and measurements at 180 cm. Unlike many applications, we limit our model to the resolution of our measurements rather than fitting polynomial functions to pCO_2 data to model depth-continuous net CO_2 production. We chose this resolution to capture the broad patterns of depth-dependent processes and thus avoid potential errors associated with polynomial or exponential fitting functions on the modeled location and magnitude of productivity, particularly near the surface (Maier & Schack-Kirchner, 2014). Additionally, fitting of polynomial functions often enforces the condition of no CO_2 consumption in the subsurface, which obscures net CO_2 drawdown processes.

For simplicity, effective diffusivity, D^*, is assumed to vary as a linear function of soil water saturation and temperature (Campbell, 1985; Steefel et al., 2015):

$$D^* = \left(1 - \frac{VWC - VWC_o}{VWC_{sat} - VWC_o}\right) * \left(\frac{T}{283}\right)^{1.75} * D \tag{4}$$

where VWC_o is the residual soil water content, assumed to be the minimum observed value across the three observational years of 0.07; VWC_{sat} is water content at saturation taken as the maximum observed value of 0.45, equivalent to porosity; T and 283 are soil and a reference temperature (K), respectively; and D is dry soil diffusivity set as 0.05 (cm/s^2) based on measured surface fluxes and pCO_2 at 25 cm over the course of our monitoring period. While the range of calculated CO_2 production values is sensitive to this dry soil diffusivity, overall patterns are not. We note that a conservative estimate of ±20% error on this D estimate would result in a relatively uniform 20% reduction or amplification of modeled production rates. For the model, we use a spatial linear interpolation and daily average of VWC to calculate D^* at the midpoint in depth between each CO_2 measurement (12.5, 37.5, 62.5, 87.5, 125, and 165 cm).

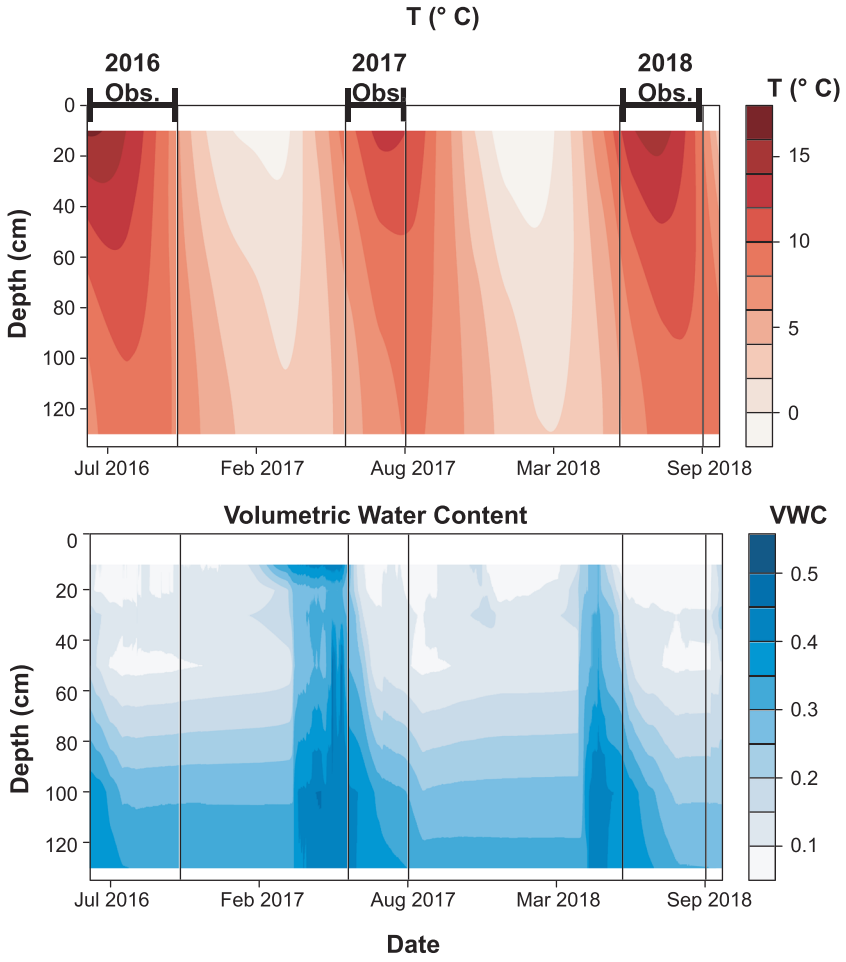

Figure 3. Depth profiles of soil temperature (top) and volumetric water content (bottom) at BM site from June 2016 through October 2018. Growing season pCO_2 observational periods are denoted with vertical lines.

3.3. Plant Phenology and Remote Sensing

Plant phenology is assessed using the enhanced vegetation index (EVI) product from publicly available MODIS13 Q1 data (Didan, 2015). MODIS data were downloaded and processed using the MODISTools package for R (Tuck et al., 2014). We analyzed EVI rather than normalized difference vegetation index (NDVI) as it corrects for variability induced by atmospheric aerosols and changes in soil reflectance. MODIS data are collected at 1–2 day intervals at a resolution of 250 m, and 16 day composites are generated from a combination of quality filtering and representative pixels. Due to the resolution of MODIS grid cells in relation to our site, we acknowledge that changing EVI may reflect changes in willow riparian zones and conifer stands, in addition to the meadow vegetation. To evaluate such bias in the MODIS data, we compared MODIS data to 30 m grid resolution Landsat-8 EVI directly over meadow vegetation at our site for years 2016–2018 (supporting information). The Landsat-derived EVI exhibits major trends in intra-annual and interannual variability comparable to MODIS data but with poor temporal resolution; thus, we present the MODIS data here.

4. Results

4.1. Soil Temp, VWC, and pCO_2

Soil temperature and VWC variability over the 3 years of observations is driven primarily by annual cycles involving the buildup of snowpack over the winter months (November–April), snowmelt in late spring, and periodic precipitation events over the course of the growing season (Figure 3). Soil temperatures at shallow depths display large diel variation (10–15°C at 10 cm tapering down to 0.5–1°C at 30 cm) over the

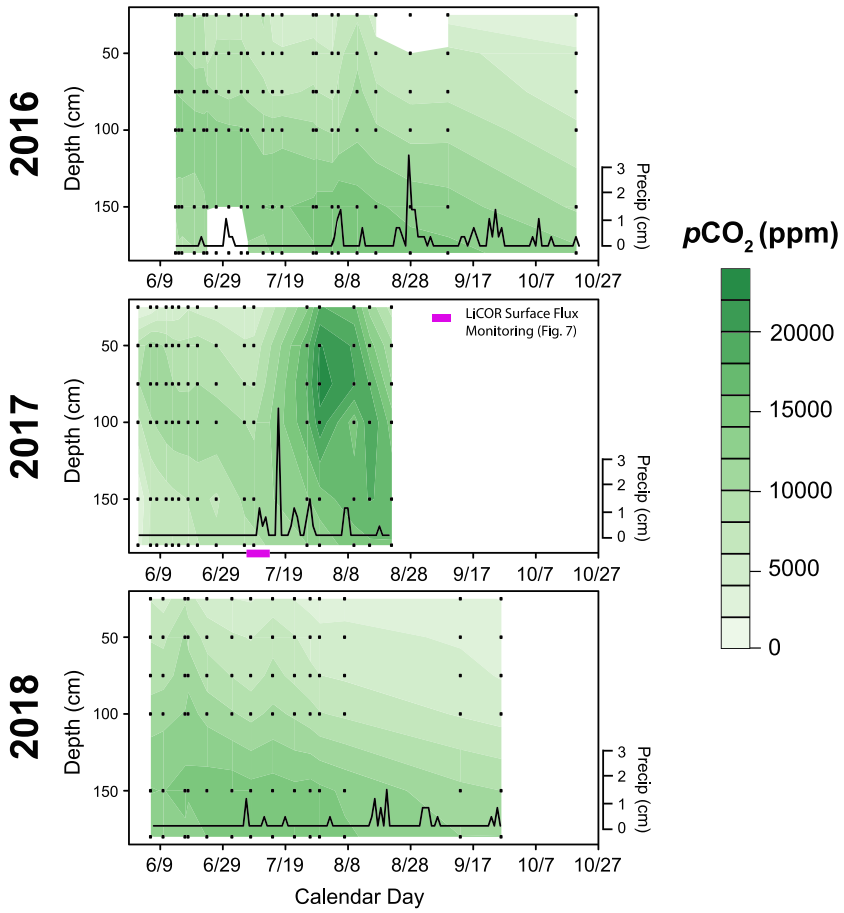

Figure 4. Depth profiles of measured pCO_2 in 2016, 2017, and 2018 (top to bottom). Color contours are based on linear interpolation between observations points (black dots). Black lines denote daily precipitation rates, to highlight pulse behavior. The purple bar in 2017 represents LiCOR flux chamber deployment for subhourly surface flux measurements.

growing season, which ceases under snow cover. Based on the emergence of diurnal temperature variability, local first snow-free days were 18 May, 24 May, and 6 May for 2016, 2017, and 2018, respectively. This matches patterns observed at the Schofield SNOTEL site described above, though shifted ~2 weeks earlier due to differences in elevation (~300 m).

Over the course of the three observational periods, daily average temperatures at 10 cm depth were similar between 2016, 2017, and 2018 at ~15°C. Average shallow soil VWC was elevated in 2017 at 0.14, reflecting the late snowmelt and persistence of wetter conditions in early June, as well as the large precipitation event in July. Shallow VWC averages were slightly lower (0.10) in 2016, and conditions were driest (average 10 cm VWC value of 0.074) in 2018.

Measured subsurface pCO_2 values across all seasons and depths ranged from 1,900–23,000 ppm (Figure 4). Across 2016 and 2017, the depth of maximum soil pCO_2 was 75–100 cm at the start of the growing season and migrated downward through the early summer. This pattern translates into increasing pCO_2 at deeper depths (130–180 cm) and decreasing pCO_2 at shallower depths (25–75 cm) through June and July. As fluxes are proportional to the concentration gradient, these trends denote net fluxes of CO_2 into the deep subsoil (>165 cm) through June and July and a switch to net CO_2 fluxes out of the deep subsoil through the late growing season. In 2017, however, the net flux of CO_2 into the deep subsoil lasted the entire observation period in response to monsoonal rain events as discussed below.

Across all three seasons, a general decline in shallow subsurface pCO_2 through the growing season was punctuated by transient increases at a range of depths, generally tied to precipitation events (black lines

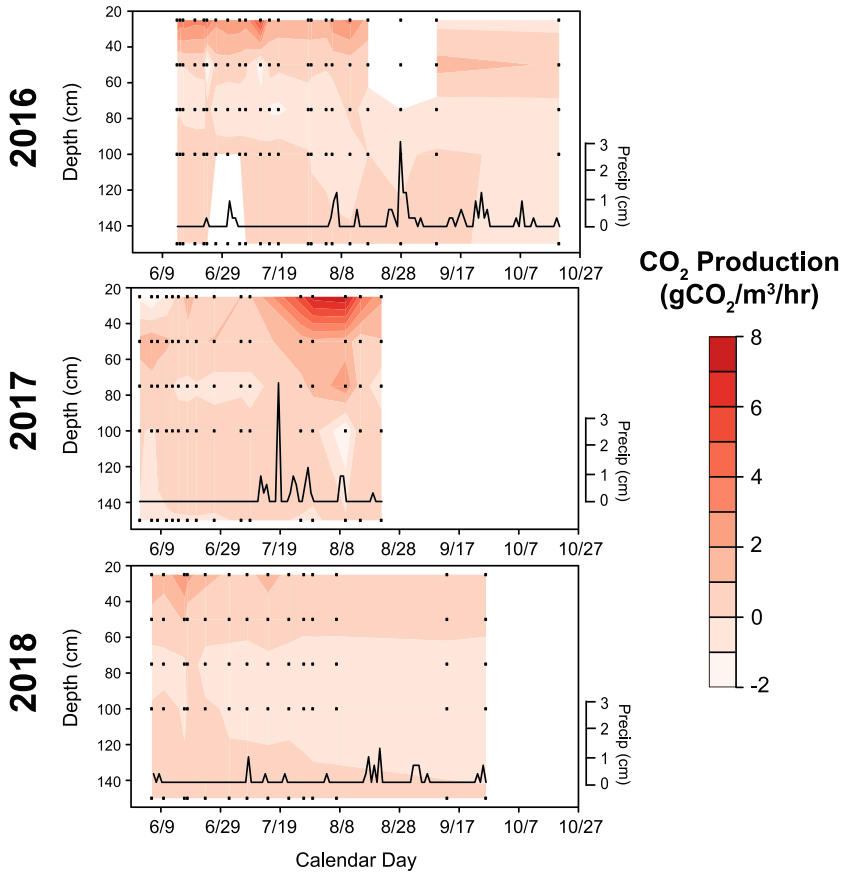

Figure 5. Depth profiles of calculated net CO_2 production rates using the steady-state diffusion-production model as described in section 3.2. Transient model output is shown for comparison in Figure S4. Negative values denote possible CO_2 consumption via advection and chemical weathering of observed calcium carbonate below ~50 cm. Black dots represent pCO_2 observation points, color contours represent linear interpolation, and the black lines denote daily precipitation rates, as in Figure 4.

in Figure 4). In 2016, this transient increase occurred in mid-August; in 2017, it occurred in late July/early August, and in 2018, two transient increases occurred in late June and mid-July. These events were similar in terms of profile characteristics and duration across 2016 and 2018, with pCO_2 increasing proportionally across all depths and lasting for one to two sampling intervals, generally on the timescale of 1 week. In contrast, the transient event in 2017 was characterized by maximum increases in pCO_2 at 75 cm, resulting in a bullseye-like pattern that did not recover to preevent values over the ensuing five sampling intervals lasting >1 month. This bullseye pattern also comprised the highest observed pCO_2 values throughout all three seasons of monitoring. Finally, late season values in September and October for 2016 and 2018 were significantly lower than growing season values at all depths except 180 cm.

4.2. Subsurface Net CO_2 Production Rates

Calculated net CO_2 production rates across the three growing seasons ranged between −2.1 and 7.9 $gCO_2/m^3/hr$, with the highest values located in the shallowest depths (Figure 5). These high shallow values are associated with lower absolute pCO_2 relative to the rest of the soil profile due to the steep gradient between subsurface and atmospheric values. Negative values occur primarily below 50 cm, coincident with the occurrence of carbonate minerals. Negative production values are also observed at 25 cm in the early season of 2017 and late season of 2016, coincident with snowmelt infiltration and a large rain event.

Shallow CO_2 production showed the highest degree of variability, primarily in response to rain events through all three growing seasons. The restriction of production responses to the shallowest depths is supported by the VWC observations, which showed little influence of summer storm events below 30 cm

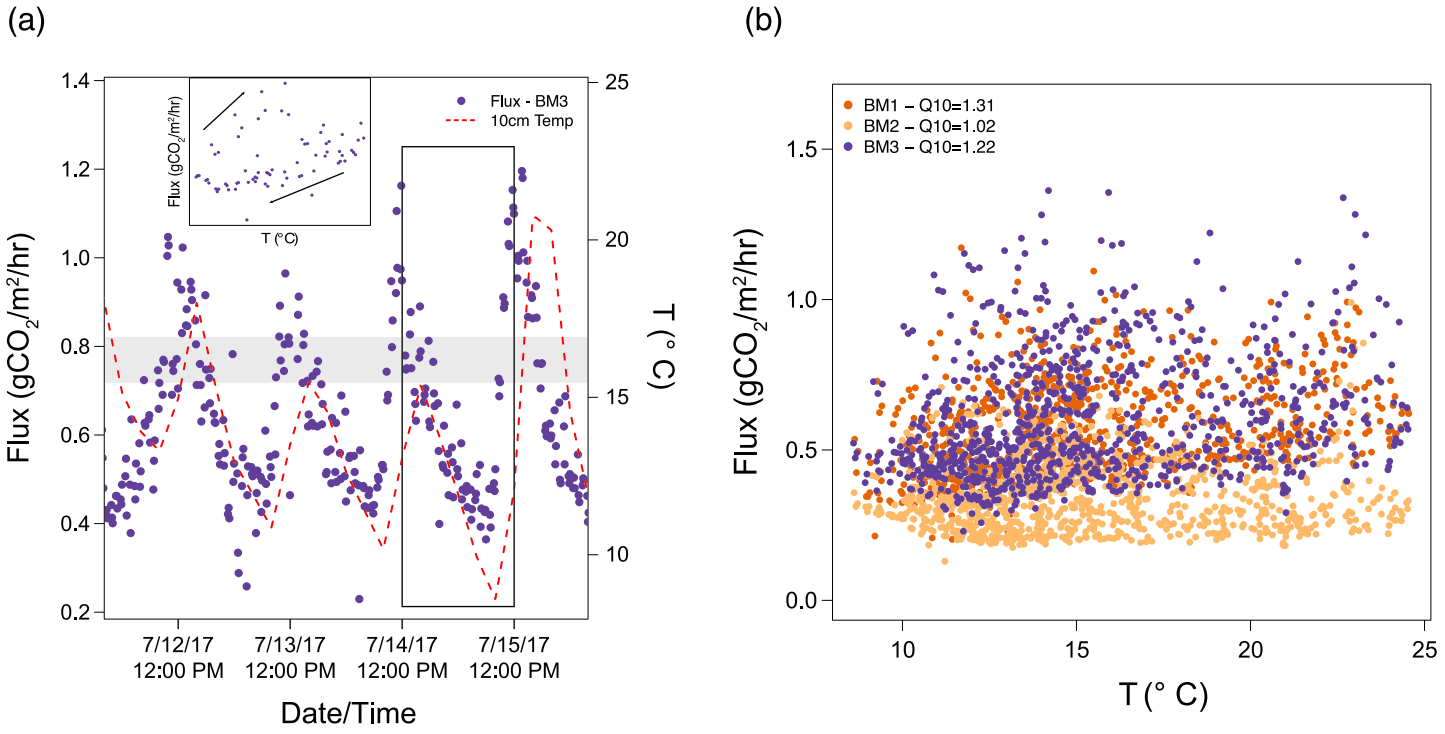

Figure 6. (a) Time series of LI-COR surface fluxes measured at BM-3 along with 10 cm soil temperature from Campbell array. Time series display phase shift in diel oscillation resulting in hysteresis in flux-temperature relationships as shown in inset. Gray shaded area represents the 2σ range of measured discrete interval EGM-5 surface fluxes from 7 July 2017 for comparison (Figures 9 and S2). (b) Temperature-flux relationships for all three chambers and 10 cm soil temperature from Campbell array with calculated Q_{10} values in legend.

(Figure 3). However, during large monsoon events in 2016 and 2017 respiration rates as deep as 50 cm increased coincident with small increases in 50 cm VWC. Notably, the response of CO_2 production rates to the large 2017 monsoon events was driven by shallow production despite the bullseye-like pattern of pCO_2 at 75 cm (Figure 4). Similar to pCO_2, elevated respiration rates persisted above preevent rates for all of the subsequent observations of 2017, spanning roughly a month. In contrast, transient increases in response to all other observed precipitation events only persisted for ~1 week. The response of shallow respiration rates to the late season monsoonal precipitation events in 2016 was markedly different in both sign and magnitude from that of 2017. In 2016 we observed negative values at 25 cm and the highest response at 50 cm.

4.3. Surface CO_2 Fluxes

High-resolution LI-COR surface flux observations in mid-July 2017 ranged from 0.13–1.36 $gCO_2/m^2/hr$ with an average of 0.50 ± 0.20 across all three sites (Figure S1). All locations showed distinct diel variability, with fluxes reaching a peak at ~14:00 MDT and a low at ~05:00 MDT. Temperature oscillations at 10 cm lagged 1–2 hr from surface fluxes at BM-3, resulting in a distinct hysteresis pattern between CO_2 flux and temperature (Figure 6). This hysteresis is commonly observed in vegetated areas and reflects the phase offset in peak autotrophic respiration from peak soil temperatures caused by root respiration and exudate release. At sites BM-1, BM-2, and BM-3, Q_{10} values based on 10 cm soil temperature were 1.31, 1.02, and 1.23, respectively (Figure 6b). These values generally correlate with field-observed moisture conditions with the driest site, BM-2, having the lowest Q_{10}. These values are on the low side of typical Q_{10} observations (~1.5–4.5) and may in part reflect the damping effect of phase-lagged autotrophic respiration.

Periodic discrete surface fluxes measured using the PP Systems EGM-5 soil respiration chamber are compared across growing seasons (Figure S2), along with shallow soil CO_2 production fluxes integrated over the shallow soil model depth to convert to units of $gCO_2/m^2/hr$. Across all three growing seasons, surface fluxes varied between 0.22 and 1.65 $gCO_2/m^2/hr$. Average CO_2 surface fluxes were 0.69 ± 0.19 $gCO_2/m^2/$

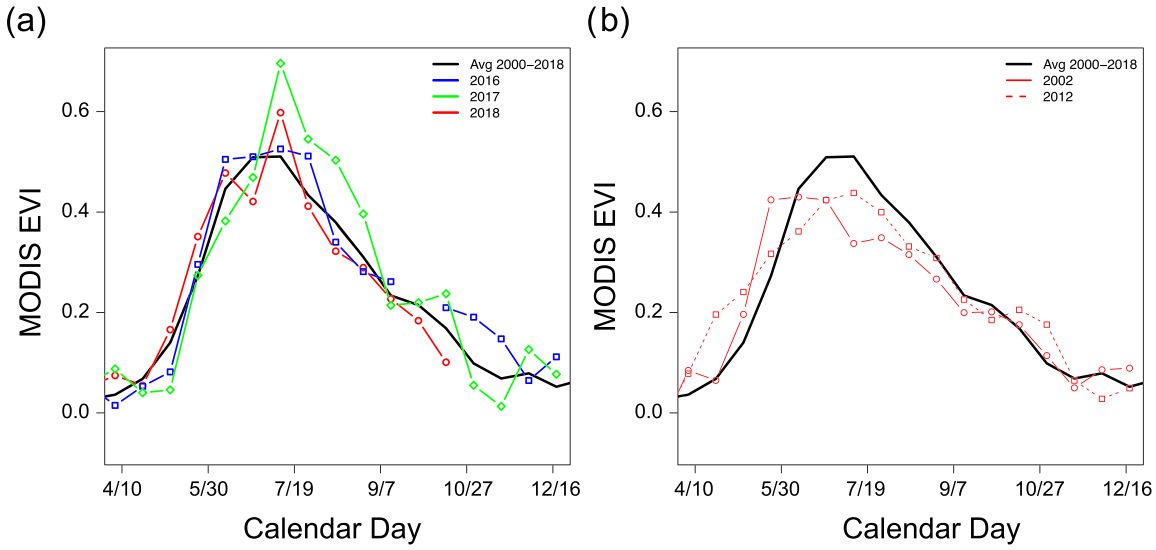

Figure 7. MODIS enhanced vegetation index (EVI) over the growing season in 0.0625 km^2 pixel encapsulating BM site for (a) 2016–2018 observational periods and 2000–2018 average values and (b) historical drought years 2002 and 2012 along with 2000–2018 average.

hr in 2016, 0.78 ± 0.36 $gCO_2/m^2/hr$ in 2017, and 0.43 ± 0.19 $gCO_2/m^2/hr$ in 2018, indicating elevated fluxes during the wettest growing season and diminished fluxes during the driest growing season. We also compare discrete EGM-5 surface fluxes from 7 July 2017 to LiCOR measurements (Figure 6a, gray shaded area), which suggests that discrete measurements are slightly elevated relative to average daily fluxes. We note that this time period also coincided with significant offsets between measured fluxes and modeled shallow soil CO_2 production (Figure S2), suggesting significant <10 cm respiration due to elevated soil moisture and small precipitation events preceding the large monsoon event. As with shallow soil CO_2 production, transient increases in surface fluxes within each growing season coincided with precipitation events and increases in soil moisture, and these transient increases did not persist for more than ~1 week. The exception to this pattern was the July 2017 monsoonal event, after which elevated surface fluxes persisted for >2 weeks. During 2016 and 2017, transient increases in surface fluxes appear to precede increases in shallow CO_2 production fluxes, potentially reflecting lagged soil moisture responses at depth and/or the downward diffusion of CO_2 produced at <10 cm depth to the 25 cm gas well. The largest offset between observed surface fluxes and calculated shallow CO_2 production occurred in the early season of 2017 and may be tied to downward advection of CO_2 by snowmelt infiltration.

4.4. Plant Phenology

Average MODIS EVI data from 2000–2018 follow a standard growing season pattern (Figure 7). Values increased starting around mid-April of each year. Peak EVI generally occurred between late June and mid-July with values of 0.51, and EVI decreased steadily starting in mid-July through early November with plant senescence, matching patterns observed in the region (Sloat et al., 2015). Over our observational period, the initial increase in growing season EVI values corresponded qualitatively with snowmelt timing based on the first snow-free day at the higher elevation SNOTEL site, with increases occurring earliest in 2018 followed by 2016 and 2017 (Figure 7a). In 2016, peak EVI values of ~0.52 occurred at the beginning of June and remained stable through mid-July. Peak EVI values were highest in 2017, reaching ~0.7 in mid-July, potentially due to a combination of the largest peak SWE and shortest fore-summer drought. In 2018, peak EVI was ~0.6; however, this peak came following a dip in EVI values in early July and may represent vegetation response to small precipitation events. Peak EVI values were greater in 2018 than 2016, yet integrated growing season EVI values were higher in 2016, reflecting longer sustained growth. While peak EVI values in 2017 and 2018 do not correspond directly with monsoonal precipitation event timing, we note again that EVI values reflect a single representative day within a 16 day timeframe, such that it is difficult to compare on short timescales.

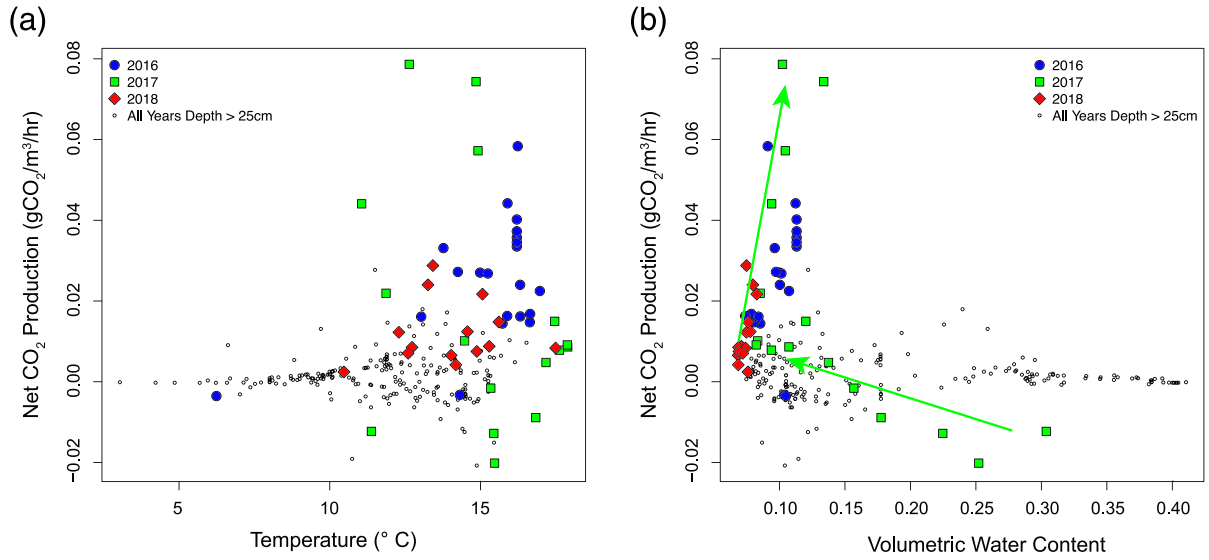

Figure 8. Relationships between net CO_2 production and (a) soil temperature and (b) volumetric water content. Shallow soil values (25 cm) are represented by larger colored markers, where color and shape represent year. All other values (depth > 25 cm) are represented by small white circles. Green arrows show temporal evolution of 2017 shallow production.

We also include EVI trends from important drought years 2002 and 2012, which have been suggested to represent future projected conditions across the Rocky Mountains (e.g., Knowles et al., 2018). Both years were characterized by lower-than-average snowpack and early snowmelt (Figure 2). As a result, EVI increases occurred earlier than average at the onset of the growing season. Peaks in EVI were also lower than average in these drought years, and senescence began particularly early in 2002.

5. Discussion

Taken together, we sought to characterize (1) trade-offs in environmental drivers of soil respiration fluxes across temporal scales, (2) the role of autotrophic responses to rain events in driving growing season soil respiration, and (3) contributions of subsoil processes to integrated soil respiration fluxes, corresponding to our stated research questions. Our main findings are summarized briefly here and are discussed in detail in the following subsections. Overall, net CO_2 production throughout the soil, as well as fluxes to the atmosphere, responded to a combination of temperature, soil moisture, and plant phenology, with each exerting influence over a unique range of timescales and depths. Although high-frequency short-term measurements of surface fluxes depend on diel temperature variations, a more complex signal is present in the average fluxes and respiration rates that points to interactions between soil moisture and vegetation status as a control on seasonal respiration rates (sections 5.1–5.3). Comparing across the 3 years of data, soil respiration and surface CO_2 fluxes responded differentially to precipitation events of similar magnitude depending on the life stage of the vegetation (i.e., actively photosynthesizing vs. senescing) (section 5.4). Drought conditions, which are projected to occur more frequently, result in decreased plant productivity and consequent reductions in overall soil respiration and autotrophic pulse responses (section 5.5). In contrast to shallow CO_2 production and surface fluxes, the deep subsoil (>165 cm) evolved from a CO_2 sink to a CO_2 source over the course of each growing season, contributing to integrated surface CO_2 fluxes (section 5.6).

5.1. Effect of Temperature on Soil Respiration and Surface Fluxes

On intra-annual and interannual timescales, temperature was not a significant driver of soil respiration or shallow net CO_2 production, as shown by the lack of any significant relationship between temperature and 25 cm CO_2 production in Figure 8a (p value > 0.3 for linear regressions within and across all three seasons). This result is similar to findings at the proximal warming meadow (Saleska et al., 2002) and in semi-arid environments more generally, where soil moisture controls tend to dominate seasonal respiration patterns (Almagro et al., 2009; Carbone et al., 2011; Hicks-Pries et al., 2017). Temperature did act as a

Table 1
Linear Regression Statistics Between Shallow Soil CO_2 Production and Environmental Drivers

	Temperature		VWC		EVI	
	r^2	p value	r^2	p value	r^2	p value
All data	0.003	0.7	0.088	0.03	0.22	0.000473
2016	0.056	0.315	0.14	0.095	0.427	0.000973
2017	0.117	0.208	0.6241/0.3[a]	0.02/0.027[a]	0.26	0.0441
2018	0.011	0.715	0.41	0.014	0.14	0.18

[a]Values excluding/including early season negative CO_2 production.

significant control on diel variability of surface fluxes, potentially modified by plant activity (Figure 6; p value < 1E−12 for BM-3 proximal to temperature sensors). Temperature also contributed to variability in net CO_2 production rates across soil depths. However, an unrealistically high Q_{10} value of 9.8 suggests that this correlation may be due to a confluence of other processes (e.g., rhizosphere respiration) that support the highest CO_2 production rates at the shallowest depths (Davidson, Janssens, & You, 2006; Davidson et al., 1998), where temperature was also highest. Across all three seasons, measured surface fluxes did not correlate with surface soil temperatures on timescales coarser than diel relationships (Table 1, p values > 0.05).

5.2. Effect of Soil Moisture on Soil Respiration and Surface Fluxes

Soil moisture acted as a primary control on surface CO_2 fluxes and shallow net CO_2 production rates, similar to findings in semiarid Mediterranean and savanna ecosystems (Carbone et al., 2011; Fan et al., 2015; Munson et al., 2010). In particular, soil respiration rates consistently increased in response to rain events under dry antecedent conditions (VWC of 0.07–0.11), with linear regression r^2 and p values shown in Table 1 within and across the 2016–2018 growing seasons. Across all three seasons, VWC was a weak but significant predictor of shallow soil CO_2 production, with particularly strong power in 2017 (excluding early season snowmelt values) and 2018 during the drought. These episodic responses contributed a significant proportion of seasonally integrated soil respiration, though precise quantification would require higher sampling frequency to capture litter and shallow (<10 cm) heterotrophic responses (e.g., Xu et al., 2004). Episodic CO_2 production exhibited significant variability in strength (Figure 8b), which may in part reflect changes in antecedent moisture conditions before rainfall events, as well as changes in sampling frequency between events. However, the large differences in CO_2 production response to the 2016 and 2017 precipitation events in terms of both magnitude and duration suggest changes in the underlying mechanisms of pulse-type behavior. We hypothesize that this difference relates to the ability of plants to respond to rainfall events based on their phenologic stage, as discussed in detail in section 5.4.

These typical responses to episodic changes in moisture are contrasted by the behavior observed in 2017 following snowmelt, in which we calculate shallow net CO_2 consumption under the highest VWC. This suggests a combination of O_2 limitations that inhibit respiration under near-saturated pore conditions, along with the potential advective transport of CO_2 during snowmelt infiltration. Additionally, across the complete range of depths and temporal observations, there was no systematic relationship between CO_2 production and soil moisture (Figure 8b), despite relatively uniform SOC content (Hsu et al., 2018). Previous incubations on soil samples from this site also displayed the strongest heterotrophic respiration response to wetting in the top 10 cm with subdued moisture sensitivity below 10 cm, likely related to microbial controls (Liu et al., 2019).

5.3. Effects of Plant Productivity on Soil Respiration and Surface Fluxes

Seasonal patterns of surface fluxes and shallow production of CO_2 broadly match EVI, with elevated background rates during June, July, and early August coinciding with increasing and peak EVI, despite low soil moisture (Figure 9). Across all three seasons, EVI was the strongest and most significant predictor variable of shallow soil CO_2 production (Table 1), though the strength and significance of correlations varied between growing seasons. Soil CO_2 production was most strongly correlated with EVI in 2016, with subsequent decreases in correlation in 2017 and 2018. The decrease in correlation in 2017 largely reflects the strong

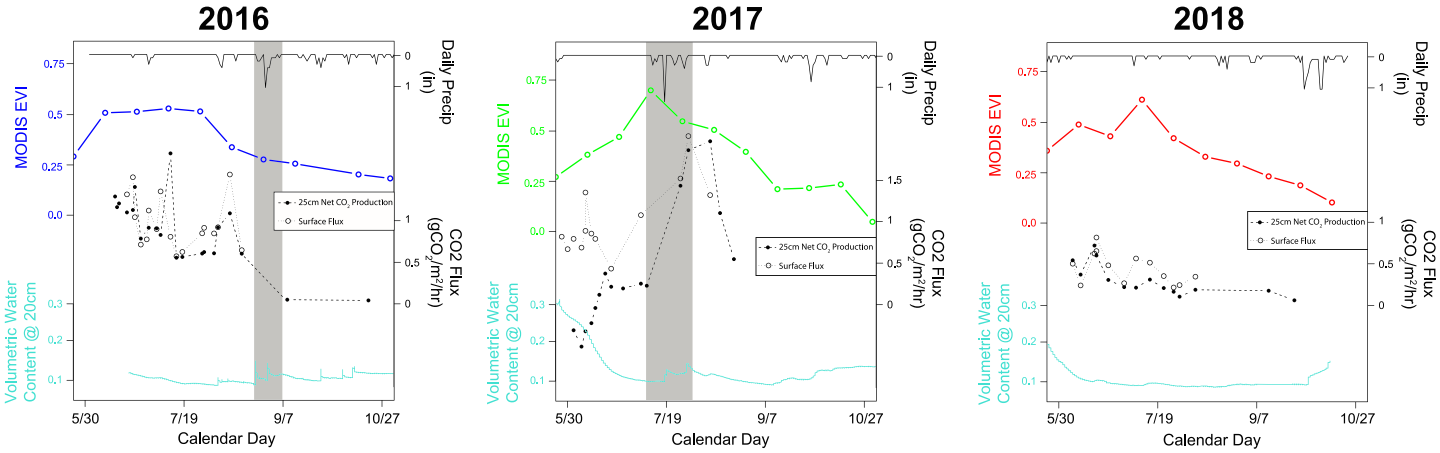

Figure 9. Growing season time series summaries for 2016–2018 (left to right), comparing relative timing from top to bottom of precipitation, MODIS EVI, CO_2 fluxes (calculated shallow production and measured surface), and 20 cm volumetric water content. The differential responses of CO_2 fluxes to the 2016 and 2017 monsoonal events are highlighted in gray.

response to the monsoon event and may also relate to low EVI temporal resolution. In 2018, the reduced correlation of EVI and CO_2 coincident with a stronger correlation between VWC and shallow soil CO_2 production suggests an important trade-off in environmental drivers under drought. This increase in correlation between soil respiration and soil moisture at the expense of EVI during drought has also been demonstrated in a deciduous broadleaf forest (Huang et al., 2014). Overall, these observations suggest that during wet, productive years, plant processes modulate soil respiration trends, whereas under less productive drought conditions, soil moisture is the primary driver of respiration trends largely through heterotrophic pulse responses to wetting.

5.4. The Role of Plant Phenology in Regulating Soil Respiration Response to Rainfall

Comparing across the 3 years of data (Figure 9), a primary signal we observed was differential responses of soil respiration and surface CO_2 fluxes to precipitation events of similar magnitude. Specifically, we noted a large and persistent response to the monsoonal rain event in July 2017, whereas we observed no elevated respiration rates following a similar event in August 2016. The large difference in responses on timescales of days to weeks suggests changes in the underlying mechanisms of respiration response. In particular, the timing of precipitation relative to background plant phenology appeared to modulate the magnitude of respiration.

The 2017 monsoonal event coincided with and likely contributed to peak EVI values, representing peak photosynthetic activity, whereas in contrast the 2016 monsoonal event coincided with lower and consistently decreasing EVI values, representing plant senescence. This suggests that the plant response to increased moisture availability during 2017 as compared to 2016 was the primary driver of these differential soil respiration signals, as supported by two primary observations.

First, the role of autotrophic respiration in driving integrated surface fluxes leading up to the 2017 event was demonstrated by hysteresis between subhourly surface CO_2 fluxes and soil temperatures at shallow depths (10–30 cm) (Figure 6). As described by a number of previous studies, this hysteresis represents a phase lag between peak temperatures and the supply of photosynthates to soil microbial communities via roots (DeForest et al., 2006; Oikawa et al., 2014; Savage et al., 2013; Tang et al., 2005). Additionally, EVI as the strongest and most significant predictor variable of shallow soil CO_2 production across all three seasons demonstrates the importance of autotrophic respiration in controlling observed soil respiration patterns.

Second, the extended duration of elevated surface fluxes and shallow soil respiration in response to the 2017 event strongly suggests autotrophic drivers. While heterotrophic respiration is sensitive to pulsed precipitation under dry conditions, rates tend to respond within hours of wetting and decrease toward preevent values as soils dry (Lee et al., 2004; Xu et al., 2004). This is generally interpreted in terms of the size and accessibility of a pool of bioavailable organic carbon that builds up under dry conditions and is quickly

depleted. Autotrophic respiration, however, tends to respond on longer timescales due to a combination of sequential lags between rain pulses, increased photosynthesis, and photosynthate supply to the subsurface observed across ecosystems (Baldocchi et al., 2006; Carbone et al., 2011; Ekblad et al., 2005; Huxman et al., 2004; Ogle & Reynolds, 2004; Williams et al., 2009). Additionally, plants may produce a protracted response to increased soil moisture availability as a result of continued photosynthesis and photosynthate supply to the rhizosphere (Huxman et al., 2004). The fact that shallow soil CO_2 production rates were elevated above preevent values in 2017 for over a month strongly suggests that autotrophic respiration was the primary driver. In contrast, the lack of elevated soil respiration rates roughly a week after the 2016 rain event suggests an insignificant autotrophic response as supported by EVI trends.

Prior studies have noted differential responses of soil respiration between the growing versus nongrowing seasons and vegetated versus nonvegetated plots. For example, Xu et al. (2004) found that the magnitude of ecosystem respiration response to precipitation events was larger at a more productive savanna grassland than at a proximal, less productive site. However, this response was interpreted in the context of heterotrophic respiration with larger available soil carbon pools, and respiration pulses decayed exponentially following wetting events in contrast to our observations. Carbone et al. (2011) quantified autotrophic responses to field wetting experiments in a Mediterranean pine forest through radiocarbon partitioning and found that autotrophic responses dominated during the growing season and were absent during the nongrowing season.

Here, to our knowledge, we present the first evidence demonstrating the importance of rain event timing relative to plant phonologic stage within the growing season itself for soil respiration rates. Comparing seasonal average surface fluxes between 2016 and 2017 suggests that the protracted 2017 response to the July monsoon resulted in an ~13% increase in CO_2 flux relative to 2016, despite similar early season values. The timing of the summer monsoon in relation to plant phenologic stage may therefore act as a primary driver of integrated growing season CO_2 fluxes. Knowles et al. (2018) recently noted significant regional increases in plant GPP across the southern Rocky Mountains in response to monsoon activity. While our site falls north of this general range, our study demonstrates that these monsoon-associated increases in GPP influence soil respiration rates as well. Our results suggest that soil respiration fluxes are more sensitive to changes in climate via the relative timing and size of precipitation in relation to plant phenology that is taken into account in typical pulse models (e.g., Fan et al., 2015; Moyano et al., 2013).

The montane plant community examined here is representative of the montane open meadow ecosystems observed throughout the Gunnison Basin (Harte, 2019; Harte & Shaw, 1995; Saleska et al., 2002; Zorio et al., 2018). Because montane ecosystems are widespread at moderately high elevations throughout North America (Vankat, 1979), their response to shifting patterns in precipitation amount and frequency is critical for understanding the ecological shifts that are occurring and their implications for carbon budgets in the region (Zorio et al., 2018). In particular, projected changes including reduced snowpack and earlier snowmelt (Clow, 2010; MRI, 2015) increase the likelihood of plant senescence preceding late season rain events, which may significantly reduce integrated soil respiration fluxes and plant inputs of carbon to soils. Assuming that autotrophic respiration implies a net input of SOC, integrated soil respiration may more directly reflect net SOC loss when plants are unable to respond to precipitation. However, countereffects such as microbial "priming" (e.g., Qiao et al., 2014; Zhang et al., 2018) and organic mineral association destabilization (e.g., Keiluweit et al., 2015) must be considered in net SOC budgets.

5.5. Soil Respiration Patterns Under Drought Conditions

Given projected changes in montane hydrology, we evaluate soil respiration trends under 2018 drought conditions within the context of plant modulation of soil respiration. Soil respiration rates and variability observed in 2018 were muted relative to 2016 and 2017. As described above, 2018 was characterized by low snowpack, early snowmelt, and relative drought throughout the growing season. These conditions contributed to earlier plant green-up and green-down. These patterns were broadly similar to those observed in 2002 and 2012, which were the two driest years within the MODIS record and have previously been used as potential near-future analog conditions (e.g., Knowles et al., 2018). Coincident with these trends, measured soil respiration rates were the lowest in 2018, reduced by almost 50% relative to 2017. Soil respiration exhibited sensitivity to precipitation events, though the magnitude of rainfall and subsequent respiration responses was small. Despite similar peak EVI values in 2018, soil respiration rates were reduced relative

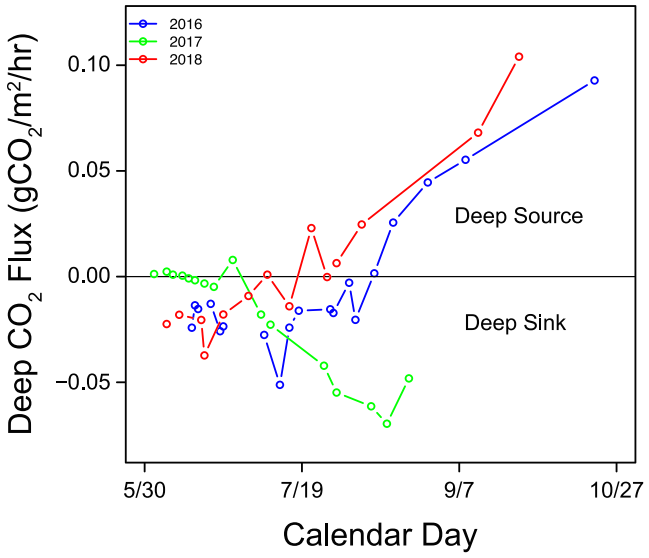

Figure 10. Calculated CO_2 fluxes based on measured concentration gradient between 150 and 180 cm observations and calculated diffusivity (Equation 4) across 2016–2018 growing seasons. Negative values denote fluxes of CO_2 into the deep subsurface, and positive values denote fluxes out of the deep subsurface. In 2016 and 2018, the deep subsurface transitions to a CO_2 source during the growing season, whereas in 2017, the large CO_2 production pulse in response to the monsoon causes the deep subsurface to remain a CO_2 sink through our observational timeframe.

to 2016. This suggests that the July 2018 rain event, despite its potential effect on peak EVI, was insufficient to cause substantial wetting at depth (Figure 9) or sustain increased autotrophic respiration. Additionally, the EVI trends during the 2012 drought indicate earlier senescence and a lower peak EVI despite significant monsoon precipitation. These observations support emerging work on the importance of snowpack amount and timing over summer precipitation in sustaining plants through times of increased water demand (Berkelhammer et al., 2020; Knowles et al., 2018; Sloat et al., 2015; Wieder et al., 2017).

These findings are also supported by observations from a long-term warming experiment that occurred roughly 3 km downvalley at a similar elevation (2,920 m), which found that drier soils caused by earlier snowmelt and increased energetic water demand led to reduced carbon inputs from plants (Saleska et al., 1999). Over the course of their experiment, soil respiration fluxes during the growing season remained relatively unchanged, potentially reflecting the competing effects of increased temperature and decreased soil moisture (Carey et al., 2016; Saleska et al., 1999, 2002). Over time, however, ecosystem-driven shifts in plant carbon inputs that were less favorable for decomposition eventually led to a recovery in SOC stocks (Harte et al., 2014).

5.6. The Subsoil as CO_2 Sink and Source

As demonstrated in the sections above, average surface CO_2 fluxes represent a range of soil processes and environmental drivers. While subsoil (>30 cm) depths display lower overall variability in CO_2 production/consumption rates, likely due to relatively stable moisture and temperature conditions, integrated rates across the subsoil contribute to observed surface fluxes. Across all 3 years of observation, calculated CO_2 production values were often negative at depths greater than ~60–100 cm and deeper. Notably, this depth range coincides with the appearance of calcium carbonate (Hsu et al., 2018), suggesting that subsurface dissolution of calcium carbonate acts as a sink for CO_2 which is converted to dissolved alkalinity (HCO_3^-, CO_3^{2-}). Additionally, we observed negative CO_2 production rates in the shallow soil (<25 cm) following the 2016 monsoon event and 2017 snowmelt, suggesting advective transport of CO_2 during infiltration events. Collectively, dissolution of calcite and vertical transport of dissolved CO_2 decouple subsurface respiration from observed surface efflux, as recently suggested by Sánchez-Cañete et al. (2018).

Additionally, the deep subsoil (>165 cm) alternates between a CO_2 sink and source over the growing season (Figure 10). In the early season, the depth of maximum pCO_2 values occurs at 75–100 cm and migrates downward over time. In 2016 and 2018, this migration resulted in a flipping of the pCO_2 gradient between 150 and 180 cm and the transition of the deep subsoil from CO_2 sink to *source*. This transition occurred in late July during 2018, and in mid-August during 2016, potentially reflecting relative snowmelt timing. In 2017, the large respiration response to the July monsoonal event resulted in the highest observed CO_2 fluxes into the deep subsoil and hindered the transition of the deep subsurface from sink to source, possibly delaying it beyond our observational timeframe. Despite the lack of direct measurements during the winter, we infer that the transition of the deep subsurface back to a sink occurs during initial snowmelt based on early season 2017 observations in which there is essentially no pCO_2 gradient at depth.

Observed maximum flux values out of the deep soil occurred in the lead-up to winter and were roughly 0.1 $gCO_2/m^2/hr$, compared to average growing season surface fluxes of 0.69, 0.78, and 0.43 $gCO_2/m^2/hr$ in 2016, 2017, and 2018, respectively. While we lack observations over the winter, taken together, these results suggest that if deep soil continues to function as a CO_2 source over the winter season, deep respiration may constitute a significant portion of annual soil respiration fluxes. This finding supports recent studies that show the deep unsaturated zone as a significant CO_2 source (Wan et al., 2018) and the transition to respiration of older carbon under insulating snowpack (Knowles et al., 2019).

Fluxes of CO_2 out of the deep subsoil likely reflect a combination of (1) redistributed CO_2 that was produced at shallow depths and diffused downward over the growing season, later resurfacing when pCO_2 gradients allowed for this CO_2 to diffuse upward; (2) oxidation of shale organic carbon; and (3) inorganic CO_2 production through the buffering of sulfuric acid from pyrite oxidation by alkalinity (Winnick et al., 2017). The disentanglement of these deep CO_2 sources is vital for constraining overall carbon budgets, as the oxidation of shale carbon and buffering of sulfuric acid are not balanced by photosynthetic inputs of carbon into the subsurface and therefore constitute a net source of carbon to the atmosphere.

6. Conclusions

To characterize the environmental controls on growing season soil respiration rates in the high elevation East River watershed, CO, we used measurements of soil pCO_2 to drive a diffusion-reaction model and calculate depth-resolved respiration patterns over the 2016, 2017, and 2018 growing seasons. These were further contextualized through comparison to subhourly chamber measurements of surface CO_2 fluxes. Across all three growing seasons, shallow CO_2 production and surface CO_2 fluxes increased in response to precipitation events and characteristic of pulse behavior. However, the response of CO_2 production rates and surface fluxes to rain events varied significantly between years, particularly in relation to the relative timing of monsoon precipitation and plant phenology. These divergent responses reflected antecedent plant phenologic stage and the ability of autotrophic respiration to respond to precipitation and soil wetting. While the role of plant phenology in modulating soil respiration pulse behavior has been demonstrated between growing and nongrowing seasons, our observations suggest that the timing of precipitation relative to phenologic stage *within* the growing season is particularly vital to predicting integrated soil respiration fluxes in montane ecosystems. Projected decreases in peak snowpack, shifts to earlier snowmelt, and increasing length and severity of the fore-summer drought in the region may therefore cause significant decreases in soil respiration fluxes through reductions in plant productivity. Additionally, earlier shifts in plant phenology may increase the likelihood of plant senescence during monsoonal rain events.

We also observed the transition of the deep subsoil (>165 cm) from a CO_2 sink to a CO_2 source in the late summer of 2016 and 2018 and inferred that this same transition was delayed in 2017 due to elevated shallow respiration in response to the monsoonal storms. If these deep fluxes persist through the winter, they would contribute a significant portion of annual fluxes from soils to the atmosphere. Quantifying the sources of this deep carbon is therefore paramount to describing integrated carbon budgets within the watershed, particularly as they may not be balanced by photosynthetic carbon uptake.

Data Availability Statement

Data generated as part of this study are archived and publicly accessible on the ESS DIVE data portal at https://data.ess-dive.lbl.gov/view/doi:10.15485/1660455 (Winnick et al., 2020), and derived data and R script used to generate figures and analyses are available in the supporting information.

Acknowledgments
We thank Kenneth Williams, Jennifer Reithel, Ian Billick, Grace Rainaldi, Hsiao-Tieh Hsu, Yuchen Liu, Sami Chen, Dana Chadwick, and the RMBL administrative staff for support in conducting this work. We also thank John F. Knowles and three anonymous reviewers for comments and suggestions that improved a previous version of this manuscript. This project was supported by funding from the U.S. Department of Energy BER Awards DE-SC0014556 and DE-SC0018155. Any use of trade, firm, or product names is for descriptive purposes only and does not imply endorsement by the U.S. Government.

References

Almagro, M., López, J., Querejeta, J. I., & Martínez-Mena, M. (2009). Temperature dependence of soil CO_2 efflux is strongly modulated by seasonal patterns of moisture availability in a Mediterranean ecosystem. *Soil Biology and Biochemistry*, *41*, 594–605. https://doi.org/10.1016/j.soilbio.2008.12.021

Baldocchi, D., Tang, J., & Xu, L. (2006). How switches and lags in biophysical regulators affect spatial-temporal variation of soil respiration in an oak-grass savanna. *Journal of Geophysical Research*, *111*, G02008. https://doi.org/10.1029/2005JG000063

Berkelhammer, M., Stefanescu, I. C., Joiner, J., & Anderson, L. (2017). High sensitivity of gross primary production in the Rocky Mountains to summer rain. *Geophysical Research Letters*, *44*, 3643–3652. https://doi.org/10.1002/2016GL072495

Berkelhammer, M., Still, C. J., Ritter, F., Winnick, M., Anderson, L., Carroll, R., et al. (2020). Persistence and plasticity in conifer water-use strategies. *Journal of Geophysical Research: Biogeosciences*, *125*, e2018JG004845. https://doi.org/10.1029/2018JG004845

Birch, H. F. (1958). The effect of soil drying on humus decomposition and nitrogen. *Plant and Soil*, *10*, 9–31. https://doi.org/10.1007/BF01343734

Bond-Lamberty, B., & Thomson, A. (2010). A global database of soil respiration data. *Biogeosciences*, *7*, 1915–1926. https://doi.org/10.5194/bg-7-1915-2010

Boone, R. D., Nadelhoffer, K. J., Canary, J. D., & Kaye, J. P. (1998). Roots exert a strong influence on the temperature sensitivity of soil respiration. *Nature*, *396*, 570–572. https://doi.org/10.1038/25119

Bradley, R. S., Keimig, F. T., & Diaz, H. F. (2004). Projected temperature changes along the American Cordillera and the planned GCOS network. *Geophysical Research Letters*, *31*, L16210. https://doi.org/10.1029/2004GL020229

Campbell, G. S. (1985). *Soil physics with BASIC* (Vol. 14, 1st ed., p. 149). Amsterdam: Elsevier. Retrieved from https://www.elsevier.com/books/soil-physics-with-basic/campbell/978-0-444-42557-7

Carbone, M. S., Still, C. J., Ambrose, A. R., Dawson, T. E., Williams, A. P., Boot, C. M., et al. (2011). Seasonal and episodic moisture controls on plant and microbial contributions to soil respiration. *Oecologia*, *167*, 265–278. https://doi.org/10.1007/s00442-011-1975-3

Carbone, M. S., & Trumbore, S. E. (2007). Contribution of new photosynthetic assimilates to respiration by perennial grasses and shrubs: Residence times and allocation patterns. *New Phytology*, *176*, 124–135. https://doi.org/10.1111/j.1469-8137.2007.02153.x

Carey, J. C., Tang, J., Templer, P. H., Kroeger, K. D., Crowther, T. W., Burton, A. J., et al. (2016). Temperature response of soil respiration largely unaltered with experimental warming. *Proceedings of the National Academy of Sciences*, *113*(48), 13,797–13,802. https://doi.org/10.1073/pnas.1605365113

Carroll, R. W., Bearup, L. A., Brown, W., Dong, W., Bill, M., & Williams, K. H. (2018). Factors controlling seasonal groundwater and solute flux from snow-dominated basins. *Hydrological Processes*, 1–16, *32*(14), 2187–2202. https://doi.org/10.1002/hyp.12151

Ciais, P., Sabine, C., Bala, G., Bopp, L., Brovkin, V., Canadell, J., et al. (2013). Carbon and other biogeochemical cycles. In T. F. Stocker et al. (Eds.), *Climate change 2013: The physical science basis. Contribution of working group I to the fifth assessment report of the Intergovernmental Panel on Climate Change* (Chap. 6, pp. 465–570). Cambridge, UK, and New York: Cambridge University Press.

Clow, D. W. (2010). Changes in the timing of snowmelt and streamflow in Colorado: A response to recent warming. *Journal of Climate*, *23*, 2293–2306. https://doi.org/10.1175/2009JCLI2951.1

Curiel Yuste, J., Janssens, I. A., Carrara, A., & Ceulemans, R. (2004). Annual Q_{10} of soil respiration reflects plant phenological patterns as well as temperature sensitivity. *Global Change Biology*, *10*, 161–169. https://doi.org/10.1111/j.1529-8817.2003.00727.x

Davidson, E. A., Janssens, I. A., & You, Y. (2006). On the variability of respiration in terrestrial ecosystems: Moving beyond Q10. *Global Change Biology*, *12*, 154–164. https://doi.org/10.1111/j.1365-2486.2005.01065.x

Davidson, E. A., Samanta, S., Caramori, S. S., & Savage, K. (2012). The Dual Arrhenius and Michaelis-Menten kinetics model for decomposition of soil organic matter at hourly to seasonal time scales. *Global Change Biology*, *18*(1), 371–384. https://doi.org/10.1111/j.1365-2486.2011.02546.x

Davidson, E. A., Savage, K. E., Trumbore, S. E., & Borken, W. (2006). Vertical partitioning of CO_2 production within a temperate forest soil. *Global Change Biology*, *12*, 944–956. https://doi.org/10.1111/j.1365-2486.2005.01142.x

Davidson, E. A., & Trumbore, S. E. (1995). Gas diffusivity and production of CO_2 in deeps soils of the eastern Amazon. *Tellus B*, *47*, 550–565. https://doi.org/10.3402/tellusb.v47i5.16071

Davidson, E. C. A., Belk, E., & Boone, R. D. (1998). Soil water content and temperature as independent or confounded factors controlling soil respiration in a temperate mixed hardwood forest. *Global Change Biology*, *4*(2), 217–227. https://doi.org/10.1046/j.1365-2486.1998.00128.x

DeForest, J. L., Noormets, A., McNulty, S. G., Sun, G., Tenney, G., & Chen, J. (2006). Phenophases alter the soil respiration-temperature relationship in an oak-dominated forest. *International Journal of Biometeorology*, *51*, 135–144. https://doi.org/10.1007/s00484-006-0046-7

Diaz, H. F., Eischeid, J. K., Duncan, C., & Bradley, R. S. (2003). Variability of freezing levels, melting season indicators, and snow cover for selected high-elevation and continental regions in the last 50 years. *Climatic Change*, *59*, 33–52. https://doi.org/10.1023/A:1024460010140

Didan, K. (2015). MOD13Q1 MODIS/Terra vegetation indices 16-day L3 global 250m SIN grid V006. NASA EOSDIS Land Processes DAAC. https://doi.org/10.5067/MODIS/MOD13Q1.006

Ekblad, A., Bostro, B., Holm, A., & Comstedt, D. (2005). Forest soil respiration rate and $\delta^{13}C$ is regulated by recent above ground weathering conditions. *Oecologia*, *143*, 136–142. https://doi.org/10.1007/s00442-004-1776-z

Ekblad, A., & Hogberg, P. (2001). Natural abundance of ^{13}C in CO_2 respired from forest soils reveals speed of link between tree photosynthesis and root respiration. *Oecologia*, *127*, 305–308. https://doi.org/10.1007/s004420100667

Fan, Z., Neff, J. C., & Hanan, N. P. (2015). Modeling pulsed soil respiration in an African Savanna ecosystem. *Agricultural and Forest Meteorology*, *200*, 282–292. https://doi.org/10.1016/j.agrformet.2014.10.009

Friedlingstein, P., Cox, P., Betts, R., Bopp, L., von Bloh, W., Brovkin, V., et al. (2006). Climate-carbon cycle feedback analysis: Results from the CMIP4 model intercomparison. *Journal of Climate*, *19*, 3337–3353. https://doi.org/10.1175/JCLI3800.1

Gaumont-Guay, D., Black, T. A., Barr, A. G., Jassal, R. S., & Nesic, Z. (2008). Biophysical controls on rhizospheric and heterotrophic components of soil respiration in a boreal black spruce stand. *Tree Physiology*, *28*, 161–171. https://doi.org/10.1093/treephys/28.2.161

Grant, R. F., & Rochette, P. (1994). Soil microbial respiration at different water potentials and temperatures: Theory and mathematical modeling. *Soil Science Society of America Journal*, *58*(6), 1681–1690. https://doi.org/10.2136/sssaj1994.03615995005800060015x

Harte, J. (2019). Chapter 1—Reflections on 27 years of manipulated ecosystem warming in a subalpine meadow. In *Ecosystem consequences of soil warming* (pp. 1–27). Amsterdam, Netherlands: Elsevier, Academic Press.

Harte, J., Saleska, S. R., & Levy, C. (2014). Convergent ecosystem responses to 23-year ambient and manipulated warming link advancing snowmelt and shrub encroachment to transient and long-term climate-soil carbon feedback. *Global Change Biology*, *21*, 2349–2356.

Harte, J., & Shaw, R. (1995). Shifting dominance within a montane vegetation community—Results of a climate-warming experiment. *Science*, *267*(5199), 876–880. https://doi.org/10.1126/science.267.5199.876

Heimann, M., & Reichstein, M. (2008). Terrestrial ecosystem carbon dynamics and climate feedbacks. *Nature*, *451*, 289–292. https://doi.org/10.1038/nature06591

Hicks-Pries, C. E., Castanha, C., Porras, R. C., & Torn, M. S. (2017). The whole-soil carbon flux in response to warming. *Science*, *355*(6332), 1420–1423. https://doi.org/10.1126/science.aal1319

Hsu, H.-T., Lawrence, C. R., Winnick, M. J., Bargar, J. R., & Maher, K. (2018). A molecular investigation of soil organic carbon composition across a subalpine catchment. *Soil Systems*, *2*(1), 23. https://doi.org/10.3390/soils2010006

Huang, N., Gu, L., & Niu, Z. (2014). Estimating soil respiration using spatial data products: A case study in a deciduous broadleaf forest in the Midwest USA. *Journal of Geophysical Research: Atmospheres*, *119*, 6393–6408. https://doi.org/10.1002/2013JD020515

Hubbard, S. S., Williams, K. H., Agarwal, D., Banfield, J., Beller, H., Bouskill, N., et al. (2018). The East River, Colorado, watershed: A mountainous community testbed for improving predictive understanding of multiscale hydrological-biogeochemical dynamics. *Vadose Zone Journal*, *17*(1), 25, 180061. https://doi.org/10.2136/vzj2018.03.0061

Huxman, T. E., Snyder, K. A., Tissue, D., Leffler, A. J., Ogle, K., Pockman, W. T., et al. (2004). Precipitation pulses and carbon fluxes in semiarid and arid ecosystems. *Oecologia*, *141*, 254–268. https://doi.org/10.1007/s00442-004-1682-4

Keiluweit, M., Bougoure, J., Nico, P., Weber, P., Pett-Ridge, J., & Kleber, M. (2015). Mineral protection of soil carbon counteracted by root exudates. *Nature Climate Change*, *5*, 588–595. https://doi.org/10.1038/nclimate2580

Knowles, J. F., Blanken, P. D., Lawrence, C. R., & Williams, M. W. (2019). Evidence for non-steady-state carbon emissions from snow-scoured alpine tundra. *Nature Communications*, *10*, 1–9.

Knowles, J. F., Molotch, N. P., Trujillo, E., & Litvak, M. E. (2018). Snowmelt-driven trade-offs between early and late season productivity negatively impact forest carbon uptake during drought. *Geophysical Research Letters*, *45*, 3087–3096. https://doi.org/10.1002/2017GL076504

Knowles, N., Dettinger, M. D., & Cayan, D. R. (2006). Trends in snowfall versus rainfall in the western United States. *Journal of Climate*, *19*, 4545–4559. https://doi.org/10.1175/JCLI3850.1

Lee, X., Wu, H.-J., Sigler, J., Oishi, C., & Siccama, T. (2004). Rapid and transient response of soil respiration to rain. *Global Change Biology*, *10*, 1017–1026. https://doi.org/10.1111/j.1529-8817.2003.00787.x

Lehmann, J., & Kleber, M. (2015). The contentious nature of soil organic matter. *Nature*, *528*(7580), 60–68. https://doi.org/10.1038/nature16069

Liu, Y., Lawrence, C. R., Winnick, M. J., Hsu, H.-T., Maher, K., & Druhan, J. L. (2019). Modeling transient soil moisture limitations on microbial carbon respiration. *Journal of Geophysical Research: Biogeosciences*, *124*, 2222–2247. https://doi.org/10.1029/2018JG004628

Maier, M., & Schack-Kirchner, H. (2014). Using the gradient method to determine soil gas flux: A review. *Agricultural and Forest Meteorology*, *192–193*, 78–95. https://doi.org/10.1016/j.agrformet.2014.03.006

Manzoni, S., Schaeffer, S. M., Katul, G., Porporato, A., & Schimel, J. P. (2014). A theoretical analysis of microbial eco-physiological and diffusion limitations to carbon cycling in drying soils. *Soil Biology and Biochemistry*, *73*, 69–83. https://doi.org/10.1016/j.soilbio.2014.02.008

Markstrom, S. L., Hay, L. E., Ward-Garrison, C. D., Risley, J. C., Battaglin, W. A., Bjerklie, D. M., et al. (2012). Integrated watershed-scale response to climate change for selected basins across the United States. (U.S. Geological Survey Scientific Investigations Report 2011–5077, p. 143).

Monson, R. K., Lipson, D. L., Burns, S. P., Turnipseed, A. A., Delany, A. C., Williams, M. C., & Schmidt, S. K. (2006). Winter forest soil respiration controlled by climate and microbial community composition. *Nature*, *439*, 711–714. https://doi.org/10.1038/nature04555

Monson, R. K., Sparks, J. P., Rosenstiel, T. N., Scott-Denton, L. E., Huxman, T. E., Harley, P. C., et al. (2005). Climatic influences on net ecosystem CO_2 exchange during the transition from wintertime carbon source to springtime carbon sink in a high-elevation, subalpine forest. *Oecologia*, *146*, 130–147. https://doi.org/10.1007/s00442-005-0169-2

Morrison, S. J., Goodknight, C. S., Tigar, A. D., Bush, R. P., & Gil, A. (2012). Naturally occurring contamination in the Mancos Shale. *Environmental Science & Technology*, *46*(3), 1379–1387. https://doi.org/10.1021/es203211z

Mote, P. W., Hamlet, A. F., Clark, M. P., & Lettermaier, D. P. (2005). Declining mountain snowpack in western North America. *American Meteorological Society*, *86*(1), 39–50. https://doi.org/10.1175/BAMS-86-1-39

Mountain Research Initiative (MRI) (2015). Elevation-dependent warming in mountain regions of the world. *Nature Climate Change*, *5*(5), 424–430. https://doi.org/10.1038/nclimate2563

Moyano, F. E., Manzoni, S., & Chenu, C. (2013). Responses of soil heterotrophic respiration to moisture availability: An exploration of processes and models. *Soil Biology and Biochemistry*, *59*, 72–85. https://doi.org/10.1016/j.soilbio.2013.01.002

Munson, S. M., Benton, T. J., Lauenroth, W. K., & Burke, I. C. (2010). Soil carbon flux following pulse precipitation events in the shortgrass steppe. *Ecological Research*, *25*, 205–211. https://doi.org/10.1007/s11284-009-0651-0

Ogle, K., & Reynolds, J. F. (2004). Plant responses to precipitation in desert ecosystems: Integrating functional types, pulses, thresholds, and delays. *Oecologia*, *141*, 282–294. https://doi.org/10.1007/s00442-004-1507-5

Oikawa, P. Y., Grantz, D. A., Chatterjee, A., Eberwein, J. E., Allsman, L. A., & Jenerette, G. D. (2014). Unifying soil respiration pulses, inhibition, and temperature hysteresis through dynamics of labile soil carbon and O_2. *Journal of Geophysical Research: Biogeosciences*, *119*, 521–536. https://doi.org/10.1002/2013JG002434

Pregitzer, K. S., King, J. A., Burton, A. J., & Brown, S. E. (2000). Responses of tree fine roots to temperature. *New Phytologist*, *147*(1), 105–115. https://doi.org/10.1046/j.1469-8137.2000.00689.x

Qiao, N., Schaefer, D., Blagodatskaya, E., Zou, X., Xu, X., & Kuzyakov, Y. (2014). Labile carbon retention compensates for CO_2 released by priming in forest soils. *Global Change Biology*, *20*, 1943–1954. https://doi.org/10.1111/gcb.12458

Raich, J. W., & Schlesinger, W. H. (1992). The global carbon dioxide flux in soil respiration and its relationship to vegetation and climate. *Tellus B*, *44*(2), 81–99. https://doi.org/10.3402/tellusb.v44i2.15428

Reichstein, M., Rey, A., Freibauer, A., Tenhunen, J., Valentini, R., Banza, J., et al. (2003). Modeling temporal and large-scale spatial variability of soil respiration from soil water availability, temperature and vegetation productivity indices. *Global Biogeochemical Cycles*, *17*(4), 1104. https://doi.org/10.1029/2003GB002035

Saleska, S. R., Harte, J., & Torn, M. S. (1999). The effect of experimental ecosystem warming on CO_2 fluxes in a montane meadow. *Global Change Biology*, *5*, 125–141. https://doi.org/10.1046/j.1365-2486.1999.00216.x

Saleska, S. R., Shaw, M. R., Fischer, M. L., Dunne, J. A., Still, C. J., Holman, M. L., & Harte, J. (2002). Plant community composition mediates both large transient decline and predicted long-term recovery of soil carbon under climate warming. *Global Biogeochemical Cycles*, *16*(4), 1055. https://doi.org/10.1029/2001GB001573

Sánchez-Cañete, E. P., Barron-Gafford, G. A., & Chorover, J. (2018). A considerable fraction of soil-respired CO_2 is not emitted directly to the atmosphere. *Scientific Reports*, *8*, 13518. https://doi.org/10.1038/s41598-018-29803-x

Savage, K., Davidson, E. A., & Tang, J. (2013). Diel patterns of autotrophic and heterotrophic respiration among phenological stages. *Global Change Biology*, *19*, 1151–1159. https://doi.org/10.1111/gcb.12108

Sihi, D., Davidson, E. A., Chen, M., Savage, K. E., Richardson, A. D., Keenan, T. F., & Hollinger, D. Y. (2018). Merging a mechanistic enzymatic model of soil heterotrophic respiration into an ecosystem model in two AmeriFlux sites of northeastern USA. *Agricultural and Forest Meteorology*, *252*, 155–166. https://doi.org/10.1016/j.agrformet.2018.01.026

Sloat, L. L., Henderson, A. N., Lamanna, C., & Enquist, B. J. (2015). The effect of the foresummer drought on carbon exchange in subalpine meadows. *Ecosystems*, *18*(3), 533–545. https://doi.org/10.1007/s10021-015-9845-1

Steefel, C. I., Appelo, C. A. J., Arora, B., Jacques, D., Kalbacher, T., Kolditz, O., et al. (2015). Reactive transport codes for subsurface environmental simulation. *Computational Geosciences*, *19*(3), 445–478. https://doi.org/10.1007/s10596-014-9443-x

Tang, J., Baldocchi, D., Qi, Y., & Xu, L. (2003). Assessing soil CO_2 efflux using continuous measurements of CO_2 profiles in soils with small solid-state sensors. *Agricultural and Forest Meteorology*, *118*, 207–220. https://doi.org/10.1016/S0168-1923(03)00112-6

Tang, J., Baldocchi, D., & Xu, L. (2005). Tree photosynthesis modulates soil respiration on a diurnal time scale. *Global Change Biology*, *11*, 1298–1304. https://doi.org/10.1111/j.1365-2486.2005.00978.x

Tuck, S. L., Phillips, H. R. P., Hintzen, R. E., Scharlemann, J. P. W., Purvis, A., & Hudson, L. N. (2014). MODISTools—Downloading and processing MODIS remotely sensed data in R. *Ecology and Evolution*, *4*(24), 4658–4668. https://doi.org/10.1002/ece3.1273

Vankat, J. L. (1979). *The natural vegetation of North America: An introduction*. New York: John Wiley.

Wan, J., Tokunaga, T. K., Dong, W., Williams, K. H., Kim, Y., Conrad, M. E., et al. (2018). Deep unsaturated zone contributions to carbon cycling in semiarid environments. *Journal of Geophysical Research: Biogeosciences*, *123*, 3045–3054. https://doi.org/10.1029/2018JG004669

Wieder, W. R., Knowles, J. F., Blanken, P. D., Swenson, S. C., & Suding, K. N. (2017). Ecosystem function in complex mountain terrain: Combining models and long-term observations to advance process-based understanding. *Journal of Geophysical Research: Biogeosciences*, *122*, 825–845. https://doi.org/10.1002/2016JG003704

Williams, C. A., Hanan, N., Scholes, R. J., & Kutsch, W. (2009). Complexity in water and carbon dioxide fluxes following rain pulses in an African savanna. *Oecologia*, *161*, 469–480. https://doi.org/10.1007/s00442-009-1405-y

Winnick, M. J., Carroll, R. W. H., Williams, K. H., Maxwell, R. M., Dong, W., & Maher, K. (2017). Snowmelt controls on concentration-discharge relationships and the balance of oxidative and acid-base weathering fluxes in an alpine catchment, East River, Colorado. *Water Resources Research*, *53*, 2507–2523. https://doi.org/10.1002/2016WR019724

Winnick, M. J., Lawrence, C. L., & Maher, K. (2020). Soil environmental conditions in the East River Watershed, CO. Development of a molecularly informed biogeochemical framework for reactive transport modeling of subsurface carbon inventories, transformations, and fluxes. Environmental System Science Data Infrastructure for a Virtual Ecosystem (ESS-DIVE) (United States). https://doi.org/10.15485/1660455

Xu, L., Baldocchi, D. D., & Tang, J. T. (2004). How soil moisture, rain pulses, and growth alter the response of ecosystem respiration to temperature. *Global Biogeochemical Cycles*, *18*, GB4002. https://doi.org/10.1029/2004GB002281

Zhang, Y.-L., Yao, S.-H., Cao, X.-Y., Rohr-Schmidt, K., Olk, D. C., Mao, J.-D., & Zhang, B. (2018). Structural evidence for soil organic matter turnover following glucose addition and microbial controls over soil carbon change at different horizons of a Mollisol. *Soil Biology and Biochemistry*, *119*, 63–73. https://doi.org/10.1016/j.soilbio.2018.01.009

Zorio, S. D., Williams, C. F., & Aho, K. A. (2018). Sixty-five years of change in montane plant communities in western Colorado, USA. *Arctic Antarctic and Alpine Research*, *48*(4), 703–722.